PHYSICAL REVIEW E **90**, 021002(R) (2014)

Stability of toroidal droplets inside yield stress materials

E. Pairam, H. Le, and A. Fernández-Nieves
School of Physics, Georgia Institute of Technology, Atlanta, Georgia 30339-0430, USA
(Received 17 June 2014; published 28 August 2014)

We study the stability of toroidal droplets inside a yield stress material. Similar to toroidal droplets in a viscous liquid, the slenderness of the torus controls whether it breaks into spherical droplets or grows thicker towards its center to coalesce onto itself and form a single spherical droplet. However, unlike tori generated in a viscous liquid, the elasticity of the outer medium can prevent either or both of these instabilities; this depends on the slenderness of the torus. Interestingly, we find that the value of the tube radius needed to prevent breakup is always larger than the value of the radius of the handle to prevent growth. This reflects the different deformations experienced by the yield stress material in either process. A simple model balancing the surface tension stress, which drives the evolution of the torus, and the yield stress, which favors its stability, accounts for all of our observations.

DOI: 10.1103/PhysRevE.90.021002 PACS number(s): 47.55.db, 47.55.df, 47.20.Gv, 83.60.Wc

Bubbles and droplets are ubiquitous in nature. Surface tension forces them to conform to a spherical geometry to minimize their surface area for a given volume [1]. As a result, droplets and bubbles with nonminimal surface shape, such as a torus, are not stable and always evolve, driven by surface tension, to a spherical shape. In the case of toroidal droplets, this evolution can happen in two ways [2]. On the one hand, the torus can break via Rayleigh-Plateau instabilities [3,4] to form a number of spherical droplets [2,5–7]; this number depends on the viscosity contrast between the toroidal and surrounding liquids. On the other hand, the handle of the torus can shrink towards the center while concomitantly the tube radius grows to form a single spherical droplet [2,8]; this instability is intrinsic to toroidal topologies and is never seen for the case of cylindrical jets. Interestingly, these two markedly different instabilities are coupled and toroidal droplets both exhibit shrinking and breaking as they evolve. It is the ratio between the inner radius, R, and the tube radius, a, of the droplet [see Fig. 1(a)], what determines its ultimate fate. For $R \ll a$, shrinking dominates, while for $R \gg a$, breaking dominates. It is when $R \approx a$ that this coupling is most appreciable [2].

Stabilization of toroidal droplets requires an opposing force to overcome both of these surface-tension-driven instabilities. Achieving this would certainly have consequences for applications such as three-dimensional (3D) printing, as one would be able to generate stable liquid structures with complex shapes. It would also be significant from a fundamental point of view, as it would allow the generation of nonminimal surface shapes that could be used, for example, to address how the topology of the bounding space affects the organization of an ordered material [9]. Recently, this stabilization has been achieved using a yield stress material as continuous phase [10,11]; these are materials that are solids for applied stresses below a critical stress, and that are liquids for stresses exceeding this critical value. Toroidal droplets, as well as droplets with an additional number of handles, were succesfully stabilized in this way. However, up to now, there is no available description of how toroidal droplets behave in yield stress materials, hampering progress towards understanding how this stabilization works and how it can be exploited.

In this Rapid Communication, we provide the rationale to understand and exploit this type of stabilization. We show that similar to toroidal droplets in a viscous liquid, a toroidal droplet in a yield stress material either breaks or shrinks. However, in this case, these instabilities are decoupled, even for $R \approx a$. Additionally, there is a threshold tube and inner radii above which the torus is stable. These critical values both increase with increasing yield stress. However, we find that the tube radius needed to prevent the breakup of the torus is always larger than the value of the inner radius needed to prevent shrinking of the torus, reflecting the different deformations experienced by the yield stress material in either situation. We rationalize the results with a simple model relying on the balance between the surface tension stress, which drives the evolution of the torus, and the yield stress, which favors its stability.

The yield stress material consists of polyacrylic acid microgels (Carbopol ETD 2020), at a concentration c between 0.1 and 1 wt %, mixed with 30 wt % ethanol, 2 wt % glycerol, and ultrapure water. We add NaOH to bring the pH to $\sim$7, where the microgels are fully swollen. In these conditions, the mixture is solidlike and optically transparent. We quantify the mechanical properties of this material by performing steady shear experiments with a stress-controlled rheometer (Anton Paar) using a cone-plate geometry (2° cone angle, 25 mm diameter). We note that the cone is sandblasted to prevent sample slippage. The experiment consists in applying a stress, τ, and measuring the strain rate, $\dot{\gamma}$. We find that the data is well described with a Herschel-Bulkley constitutive equation [12]: $\tau = \tau_{y,s} + k\dot{\gamma}^n$, where $\tau_{y,s}$ is the shear yield stress, k is the so-called consistency index, and n is the shear exponent. Furthermore, we find that $n \approx 0.5$ irrespective of the Carbopol concentration, indicating that the flow behavior corresponds to shear thinning; note that $n = 1$ implies viscous flow. In contrast, $\tau_{y,s}$ depends on c almost linearly [13]. Since $\tau_{y,s}$ corresponds to the shear stress value below and above which the material behaves as an elastic solid or macroscopically flows, respectively, we can tune the threshold between solidlike and liquidlike behaviors by tuning c.

We inject 10 cSt PDMS oil through a metallic needle into a rotating bath containing the yield stress material. As a result of the imposed rotation the injected liquid is able to flow through the continuous phase to form a curved jet that closes into a torus after one full revolution. The tube radius can then be controlled

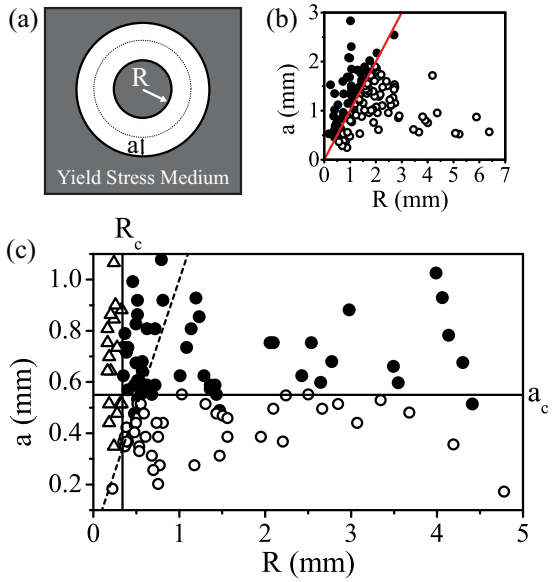

FIG. 1. (Color online) (a) Tube radius, a, and inner radius, R, of a toroidal droplet. (b) State diagram for the transformation of toroidal droplets in viscous liquids. The line $a = R$ separates regions where the torus either shrinks (closed symbols) or breaks (open symbols). Injected liquid: 10 cSt PDMS oil. Continuous phase: water with 60 mM of the surfactant sodium dedecyl sulphate. (c) State diagram for the transformation of toroidal droplets inside yield stress materials. In addition to the $a = R$ dashed line, there is a horizontal and a vertical line separating regions where the torus is stable (•) from regions where the torus either breaks (○) or shrinks (△). Injected liquid: 10 cSt PDMS oil. Continuous phase: yield stress material with $c = 0.3$ wt %, corresponding to $\tau_{y,s} = 9$ Pa.

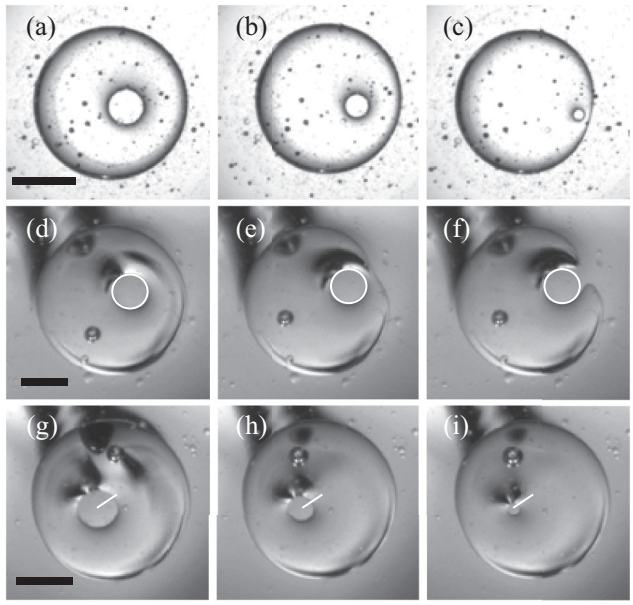

FIG. 2. Evolution of a torus: (a)–(c) Toroidal droplet made of water undergoing both breaking and shrinking simultaneously inside a 30 000 cSt PDMS oil. (d)–(f) Toroidal droplet made of 10 cSt PDMS oil undergoing only breaking inside a yield stress material with $c = 0.1$ wt %. Note that the handle does not shrink while it moves to the side to induce breakup. (g)–(i) Toroidal droplet made of 10 cSt PDMS oil undergoing only shrinking inside a yield stress material with $c = 0.1$ wt %. Note that the handle shrinks while remaining stationary. Scale bar: 5 mm.

by varying the amount of injected liquid, while the inner radius can be changed by changing the distance between the needle and the rotation axis. Thus, the formation of the toroidal droplet essentially happens as if it were made inside a viscous liquid [2]. The subsequent evolution also exhibits features that are similar to the observed evolution inside viscous liquids. Recall that in this case, the boundary separating the occurrence of breaking from shrinking is a straight line corresponding to $R = a$, as shown in Fig. 1(b). This condition is reminiscent to the Plateau criterion for the breakup of cylindrical jets, where a jet of radius a will only break if its length L is equal or longer than its own circumference, $2\pi a$. In the case of a torus, breakup only happens if $R \geqslant a$, corresponding to the Plateau criterion provided the relevant length of the torus is $L = 2\pi R$. As a result, an unstable Rayleigh-Plateau mode can only grow provided the inner perimeter of the torus is larger than the length of the circumference of the tube.

For toroidal droplets with tube radius smaller than a critical tube radius a_c, or with an inner radius smaller than a critical inner radius R_c, the droplet is unstable and either breaks or shrinks, respectively, consistent with the behavior observed for toroidal droplets inside a viscous liquid. However, while for toroidal droplets in viscous liquids these two instabilities are coupled, hence implying both a decrease in R and a as the droplet evolves, as shown in Figs. 2(a)–2(c) and the Supplemental Material, video 1 [13], this is not observed in the presence of a yield stress material. In this case, when the torus breaks, the inner circumference moves with a constant R, as shown in Figs. 2(d)–2(f) and the Supplemental Material, video 2 [13], and when it shrinks, the inner circumference contracts while its center remains stationary, as shown in Figs. 2(g)–2(i) and the Supplemental Material, video 3 [13]. Furthermore, in the presence of a yield stress material, the toroidal droplet can be stable against both types of instabilities for certain ranges of a and R. This region is bounded by a vertical line, corresponding to a critical inner radius R_c, and a horizontal line, corresponding to a critical tube radius a_c. For $R > R_c$ and $a > a_c$, the toroidal droplet is stable, as shown in Fig. 1(c). In contrast, for $a < a_c$ or $R < R_c$, it either breaks or shrinks.

Since these new boundary lines are only observed in the presence of the yield stress material, their origin must be related to the elasticity of these type of materials for applied stresses below the yield stress. Let us first consider the case of a toroidal droplet prone to breakup. Since the droplet evolution is driven by surface tension, we hypothesize that the stability threshold for breaking results from the balance of the yield stress and the surface tension stress. Hence, the critical tube radius would be determined by the condition $\tau_{y,s} = \gamma/a_c$, where γ is the surface tension. This implies that materials with a larger shear yield stress would succeed in stabilizing thinner toroidal droplets. To test this, we generate *state* diagrams like those in Fig. 1(c) for different values of $\tau_{y,s}$. We find that the boundary between stable and breaking tori shifts to higher $1/a_c$ with increasing $\tau_{y,s}$, as shown in Fig. 3 and consistent with our hypothesis. Furthermore, we find that the straight line in this plot separating these situations has a slope of 7 mN/m. Based

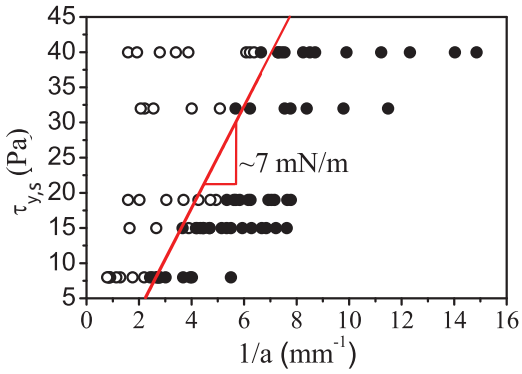

FIG. 3. (Color online) Stability diagram for thin toroidal droplets made with 10 cSt PDMS oil inside yield stress materials with different $\tau_{y,s}$. The line separates stable (open symbols) and breaking (closed symbols) tori.

on our simple model, this should be equal to the interfacial tension between the oil making the torus and the continuous phase. Using the pendant drop method [14], we determine that $\gamma = 6.6$ mN/m for these materials, further confirming our hypothesis.

Similar results are obtained with regard to the boundary line separating stable and shrinking toroidal droplets. However, in this case the relevant surface tension stress is given by γ/R_c. Interestingly, we systematically find that for a given shear yield stress, $a_c > R_c$; this is seen in Fig. 1(c) for $\tau_{y,s} = 9$ Pa, where $a_c = 0.55$ mm and $R_c = 0.34$ mm. To understand the difference in critical tube and inner radii, we consider how the continuous phase deforms for a shrinking and a breaking toroidal droplet. For shrinking, the outer material within the inner ring of the torus experiences a largely extensional flow, as schematically illustrated in Fig. 4(a) with a side view of the situation. As a result, shrinking can only happen if the normal stress due to surface tension, $T_{yy} - T_{xx} = \gamma/R$, is greater than the elongational yield stress, $\tau_{y,e}$. For breaking, however, the outer material near the torus in the region where the tube pinches experiences a deformation involving large shear contributions, as schematically illustrated in Fig. 4(b) with a top view of the situation. As a result, breaking will happen if the shear stress T_{xy} is greater than approximately the shear yield stress $\tau_{y,s}$. For Herschel-Bulkley materials [15–17] $\tau_{y,e} = \sqrt{3}\tau_{y,s}$, indicating that $\tau_{y,e}$ is larger than $\tau_{y,s}$ by a factor $\sqrt{3}$ and reflecting the fact that most materials are more easily sheared than they are elongated. We note that this relationship has been experimentally confirmed in experiments addressing the extrusion of Carbopol suspensions from a circular orifice [17,18]. If we now replace the relevant yield stress with the corresponding surface tension stress, $\tau_{y,e} = \gamma/R_c$ or $\tau_{y,s} = \gamma/a_c$, we obtain that $a_c = \sqrt{3}R_c$. This explains that $a_c > R_c$ for $\tau_{y,s} = 9$ Pa. To further test the model expectations, we determine the critical tube and inner radii, for different $\tau_{y,s}$, and plot a_c as a function of R_c. We find that they are both linearly related, as shown in Fig. 4(c), with a slope that is equal to 1.85, which is close to $\sqrt{3}$, confirming our interpretation of the results. Hence, the yield stress material deforms differently depending on whether the toroidal droplet breaks or shrinks. Furthermore, note that this difference also

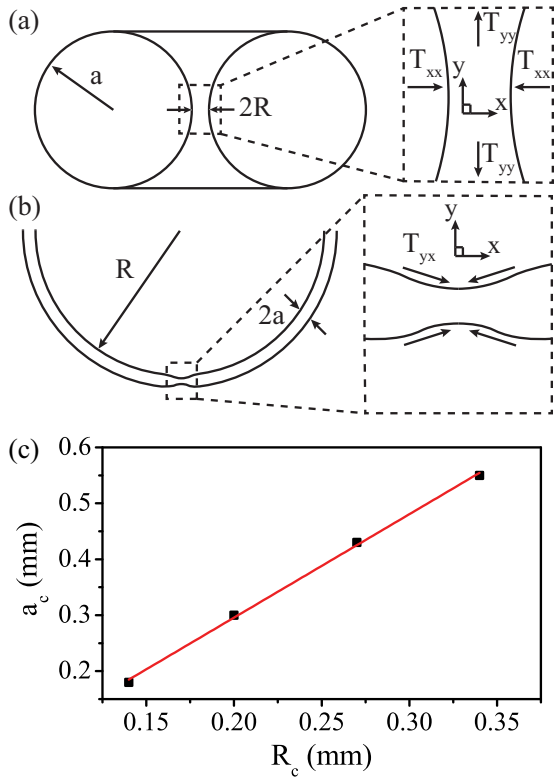

FIG. 4. (Color online) (a) Side view of a shrinking torus. The box highlights the region where the yield stress material is elongated. (b) Top view of the breaking torus. The box highlights the region where the yield stress material is sheared. T_{ij} represents the stress along the j direction acting on a surface element with normal along the i direction. (c) Critical tube radius a_c versus critical inner radius R_c. The line is the linear fit of the experimental points.

explains the observed decoupling of these instabilities in the presence of a yield stress material. This happens for $a < a_c$ and $R > R_c$, as well as for $R < R_c$ and $a > a_c$, which span the majority of the state diagram in Fig. 1(c).

A further demonstration of the stabilization effects of the yield stress material comes from the fact that a broken torus inside this material does not evolve into a spherical droplet, as it would if it were inside a viscous liquid. Instead, the toroidal droplet retracts by a given amount after breakup to adopt a crescent shape, as shown in Figs. 5(a) and 5(b). The observed retraction happens at constant volume and hence implies a growth in the tube radius. We can understand the observed stability by recalling our simple stress balance: retraction happens until the tube radius of the crescent-shaped droplet equals the critical tube radius for tori made in yield stress materials with the same $\tau_{y,s}$. To more quantitatively test this, we generate tori with different R and a within the breaking region of the state diagram and monitor their evolution after breakup inside a yield stress material with $\tau_{y,s} = 9$ Pa. At equilibrium, we determine the radius a_t of the osculating circle in the region of highest curvature. We emphasize this since the tube radius is not completely constant along the equilibrium shape. It is always highest at the ends of the crescent-shaped droplets, corresponding to the regions where the torus pinched. Since there are two of these regions, as shown in Fig. 5(b), we

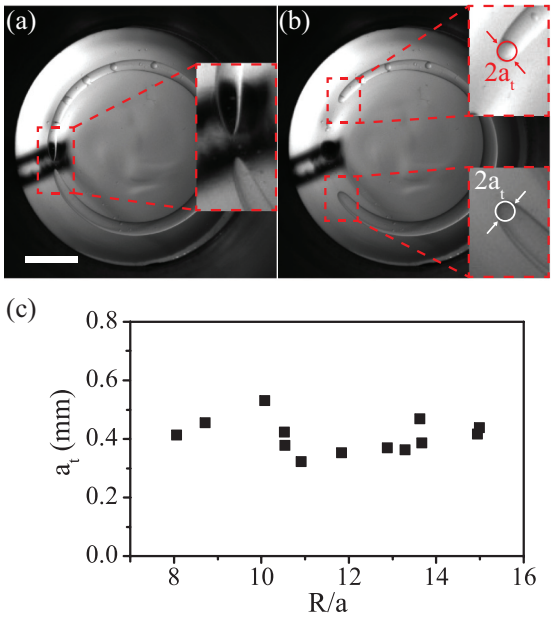

FIG. 5. (Color online) Snapshots of a toroidal droplet (a) right after breaking and (b) after equilibrated. We note that we waited for 12 hours in order to guarantee that the droplet had reached its final equilibrium shape. Beyond this time, we did not detect any further droplet evolution. The insets in (b) highlight the osculating circles used to determine the smallest tube radius of the equilibrium droplet. Scale bar: 5 mm. (c) Average radius of the osculating circles fitted at the ends of the droplet in the final crescentlike shape, a_t, as a function of the ratio R/a of the toroidal droplet before breakup. Continuous phase: yield stress material with $c = 0.3$ wt %.

take the average of the two measurements. We find that a_t is independent of the torus geometry, as shown in Fig. 5(c), consistent with the expectation that the torus will retract by the needed amount to fulfill that $a_t = a_c$. Furthermore, we obtain that $a_t = 0.45 \pm 0.09$ mm, which is essentially equal to a_c for $\tau_{y,s} = 9$ Pa. These results confirm that the key to the observed stability is the balance between the surface tension stress and the yield stress of the surrounding material.

We have demonstrated that it is possible to generate and stabilize a toroidal droplet inside a yield stress material. By tuning the yield stress of this material we can control the geometry of the torus that can be stabilized. We find that the torus is stable against breaking if its tube radius is larger than the critical tube radius, $a_c = \gamma/\tau_{y,s}$, and stable against shrinking if its inner radius is larger than the critical inner radius, $R_c = \gamma/\tau_{y,e}$, where $\tau_{y,s}$ and $\tau_{y,e}$ are the shear and elongational yield stresses of the surrounding material. The values of these length scales are different in our experiments reflecting that $\tau_{y,e} \neq \tau_{y,s}$ for our material. This difference depends on the constitutive equation of the yield stress material and determines the ratio between a_c and R_c. From our investigations, we also find that an unstable toroidal droplet in a yield stress material evolves via breaking or shrinking when $a < R$ or $a > R$, respectively. However, unlike a torus inside of a viscous medium, these distinct instabilities are decoupled inside a yield stress material. This can ultimately be traced back to the different flow behaviors that are dominant in either situation. While the relevant distortion of the yield stress material for a shrinking toroidal droplet relates to the elongation of the material near the handle, for a breaking toroidal droplet, it is the shear experienced by the surrounding material around the pinching region that is most relevant.

Our results provide the path to print stable structures inside yield stress materials with exotic shapes, as we have illustrated with the generation of crescent-shaped droplets. It is the elasticity of the surrounding medium and the existence of a yield stress that allows for printing these stable structures. This will not only be relevant for generating droplets to address fundamental questions, as recently demonstrated [11], but can also result in an all together new 3D printing technology based on yield stress materials with the potential for generating novel biological constructs [10].

We acknowledge financial support from NSF (Grant No. DMR-0847304).

[1] C. V. Boys, *Soap Bubbles: Their Colours and the Forces which Mould Them* (Dover, New York, 1959).
[2] E. Pairam and A. Fernández-Nieves, Phys. Rev. Lett. **102**, 234501 (2009).
[3] L. Rayleigh, Philos. Mag. Ser. 5 **34**, 145 (1892).
[4] S. Tomotika, Proc. R. Soc. London, Ser. A **150**, 322 (1935).
[5] H. Mehrabian and J. J. Feng, J. Fluid Mech. **717**, 281 (2013).
[6] J. D. McGraw, J. F. Li, D. L. Tran, A. C. Shi, and K. Dalnoki-Veress, Soft Matter **6**, 1258 (2010).
[7] B. D. Texier, K. Piroird, D. Quere, and C. Clanet, J. Fluid Mech. **717**, R3 (2013).
[8] Z. Yao and M. J. Bowick, Eur. Phys. J. E **34** (2011).
[9] M. J. Bowick and L. Giomi, Adv. Phys. **58**, 449 (2009).
[10] A. Fernandez-Nieves, T. Angelini, Y-W. Chang, and S. Marquez, Invention disclosure UF# 15225, 2014.
[11] E. Pairam, J. Vallamkondu, V. Koning, B. C. van Zuiden, P. W. Ellis, M. A. Bates, V. Vitelli, and A. Fernandez-Nieves, Proc. Natl. Acad. Sci. USA **110**, 9295 (2013).
[12] W. H. Herschel and R. Bulkley, Kolloid-Z. **39**, 291 (1926).
[13] See Supplemental Material at http://link.aps.org/supplemental/10.1103/PhysRevE.90.021002 for steady-state rheology data and supplementary videos 1, 2, and 3.
[14] F. K. Hansen and G. Rødsrud, J. Colloid Interface Sci. **141**, 1 (1991).
[15] C. R. Beverly and R. I. Tanner, J. Rheol. **33**, 989 (1989).
[16] C. W. Macosko, *Rheology Principles, Measurements, and Applications* (VCH Publishers, Weinheim, Germany, 1994).
[17] P. Coussot and F. Gaulard, Phys. Rev. E **72**, 031409 (2005).
[18] G. German and V. Bertola, Phys. Fluids **22**, 033101 (2010).